This is a repository copy of *Position Tracking of a Passive Rehabilitation Robot*.

Position Tracking of a Passive Rehabilitation Robot

Kazimierz K. Wojewoda, Peter R. Culmer, Andrew E. Jackson and Martin C. Levesley
School of Mechanical Engineering
University of Leeds
Leeds, UK

Abstract— This paper presents a position tracking system for real-time position estimation of a passive rehabilitation robot. The table-top robot shall be used for upper limb rehabilitation by stroke patients. Accurate estimates of the robot's position are determined by fusing data from two sensors: a laser optical sensor and a webcam. The laser optical sensor is mounted underneath the robot and tracks the motion of the robot relative to the surface on which the robot is used. The webcam is positioned above the robot and mounted on a stand fixed to the surface. The webcam detects the robot's motion relative to a fixed absolute coordinate system and supplies data at a lower frequency than the optical sensor. A data fusion scheme is implemented and validated in experiments where markers are moving along circular and pentagram trajectories. After the fusion is completed, a Kalman filter is implemented to investigate if it can improve the accuracy of the fusion tracking system. The results demonstrate that the developed fusion position tracking system can reliably track the robot's position with greater accuracy than would be possible with the webcam or the optical sensor tracking systems on their own.

Keywords— sensor fusion, position tracking, passive rehabilitation, Kalman filter.

I. Introduction

Each year there are 110,000 cases of stroke reported in England. The estimated direct cost of stroke in 2008-2009 was at least £3 billion and the wider economical cost resulting from stroke cases was estimated to be £8 billion. Stroke is the single largest cause of adult disability in England, and approximately 300,000 people are living with post–stroke complications. These numbers are likely to increase as the population ages [1].

One of the state–of–the–art and rapidly developing technologies in post-stroke recovery therapies is robotic rehabilitation. A robot-assisted therapy has many advantages over hands–on, manual therapy. Robotic systems can monitor movements and measure motor skills and can deliver coherent training during each session [2][3]. Advances in robotic technology have resulted in the development of several advanced active robotic systems for upper limb post-stroke rehabilitation. Systems such as ARMin [4], MIT-Manus [5], GENTLE/s [6] and iPAM [7] have been developed to enhance, assist and assess arm rehabilitation. There is evidence that the use of these systems can contribute to a reduction in upper limb impairment in stroke patients. However, most of these devices are not used on a mass scale due to cost, complexity and a lack of comprehensive clinical trials [8].

Robotic rehabilitation systems can be used to promote rehabilitation beyond the hospital stay. Nowadays, despite an initial hospital-based post-stroke rehabilitation being intensive, patients generally do not achieve their full recovery potential. This happens because after being discharged from hospital patients do not receive proper rehab training, which is mainly due to economic pressure and a lack of qualified human resources [8]. In order to enable patients to continue rehabilitation training at home, without the supervision of a qualified physiotherapist, a number of passive rehabilitation systems have been developed (e.g. balanced forearm orthosis and mobile arm support). However, these devices have many limitations, such as difficulty in adjusting the levels of support and resistance. Generally, they do not monitor the movements; hence they do not provide recovery feedback [9]. A novel approach to home-based arm and shoulder rehabilitation are table-top, low-cost devices such as the Arm Skate [10], ARMassist [11] and Reha-Maus [12]. All three of these devices are designed to support therapist-independent rehabilitation protocols incorporating computer games, which have been proven to maximize patient attention and therapy outcomes [13]. In order to monitor the patient's performance during the exercise (or game), each of the aforementioned table-top devices includes a system estimating their position on the table. The Arm Skate uses a webcam to determine the absolute position of the robot. The ARMassist incorporates two subsystems to determine the position and the orientation of the robot: an absolute tracking system based on an optical mouse sensor and a relative tracking system based on two mouse optical sensors. Similarly, the Reha-Maus uses two subsystems to track its position: an absolute tracking system based on an infrared camera mounted on the ceiling and a relative tracking system based on incremental encoders measuring rotations of wheels mounted underneath the robot. The Reha-Maus uses a modified Kalman filter to fuse data from the two subsystems.

In this paper, a novel position tracking system fusing position data from a webcam (absolute tracking) and an optical mouse sensor (relative tracking) is presented and experimentally evaluated. Position data from the webcam and the optical mouse sensor is fused to provide more accurate position estimates than would be possible using these sensors on their own. The developed tracking system can be used to track the position of a passive rehabilitation joystick, which is shown in Figure 1. The joystick is intended for use on a table top, with rehabilitation tasks displayed on a monitor. The two main subsystems are the low-cost position tracking system and the guiding system. The guiding system directs the patient's movements in the correct direction. The position tracking

system is introduced in this paper. Its objective is to monitor the trajectory of the patient's movements in order to monitor the progress of their rehabilitation therapy.
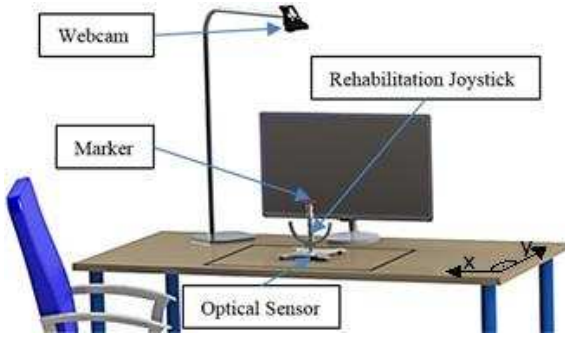

Fig. 1. Conceptual setup of a passive rehabilitation joystick system.

II. POSITION TRACKING SYSTEM

The developed position tracking system consists of two independent subsystems whose measurements are fused together. These two subsystems are: an absolute position tracking system, and a relative position tracking system, the main components of which are a webcam and an optical sensor respectively. The absolute position tracking system is based on a webcam mounted on a fixed stand and tracking a marker moving underneath it. The webcam detects the motion of the moving marker relatively to a fixed coordinate system. The relative position tracking system is based on a mouse laser optical sensor which is attached to the tracked object. The laser optical sensor detects motion relatively to the surface on which it is being used. A suggested fusion scheme, described later, combines position data acquired from the webcam and the optical sensor in order to obtain higher precision position estimates than would be possible if the systems were used on their own. Data sampling time is different and unsteady for both the webcam and the optical sensor. The optical sensor sampling frequency is assumed to always be faster than the sampling frequency of the webcam. A fusion trajectory is based on optical sensor measurements and the webcam measurements are utilized to correct the drift inherent to the optical sensor.

A schematic diagram of a proposed fusion scheme is presented in Figure 2. The webcam acquires low-update-rate absolute position measurements which are subject to noise corruption. The optical sensor acquires fast-update-rate position measurements which are subject to drift affecting tracking accuracy. Position measurements acquired from the webcam and optical sensor are fused together utilizing the fusion scheme presented in this section. In the last step fused data which is partially noise-corrupted is filtered using a discrete Kalman filter.
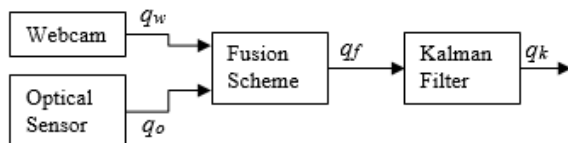

Fig. 2. Schematic diagram of the fusion scheme.

A. Fusion scheme: A case when webcam data is not available.

If the webcam data is not available the following equation was used to calculate the position:

$$q_f(t) = q_f(t-1) + \Delta q_o(t) \tag{1}$$

q_f is the fused position, Δq_o is an optical sensor-measured position increment from the most recent position measurement and t is the time when the measurement was taken.

B. Fusion scheme: A case when webcam data is available.

When webcam position measurements q_f are present the position is calculated as follows:

$$q_f(t) = q_f(t-1) + \Delta q_o(t) + w \times C(t_w) \tag{2}$$

where w is a weight, C is a position correction term and t_w is a time when webcam measurements are available. The correction term C is calculated according to:

$$C(t_w) = q_w(t_w) - q_f(t_w) \tag{3}$$

q_w is a position measurement from the webcam. q_f was interpolated at t_w, for each iteration t_w satisfies

$$t_w \leq t \text{ and } t_w > t - 1 \tag{4}$$

Instead of adding the correction term C in one t time step to compute position results, it was divided by eight and added eight times. This approach minimises sudden sharp changes on a trajectory graph. Implementing the correction C over eight steps was done as the minimum measured number of measurements acquired by the optical sensor between two webcam position measurements was eight.

The gain w is calculated based on an average strength (AS) parameter measured by the webcam. Average strength is a gradient magnitude of the detected edge (of the tracked marker) and it was measured on a scale from 0 to 1. The gain w was calculated using the following formulas:

$$w = 0, \text{ for } AS < 0.90$$
$$w = 6.25 \times AS - 5.125, \text{ for } AS \geq 0.90 \text{ and } AS < 0.98 \tag{5}$$
$$w = 1, \text{ for } AS \geq 0.98$$

C. Kalman filter.

The type of the Kalman filter used is a discrete Kalman filter which was applied to the fused position data [14]. The Kalman filter was designed to estimate the state of a discrete-time controlled process that can be described by the use of a stochastic difference equation

$$x_k = Ax_{k-1} + Bu_k + w_{k-1} \tag{6}$$

with a stochastic output equation

$$z_k = Hx_k + v_{k-1} \tag{7}$$

where x_k is the process state and z_k is the process measurement at the step k. The variable w_k is the process noise and the variable v_k is the measurement noise. H is a matrix of compatible dimension that relates the state to the output. u_k is the optional control input. A and B are matrices that govern the dynamic behaviour of the system.

Assuming that Q and R are the process noise covariance and the measurement covariance, the recursive discrete Kalman filter algorithm can be written with the following five equations:
1) Time update equations
   a) A state prediction:
       $$\hat{x}^-_k = A\hat{x}_{k-1} + Bu_k$$
   b) Prediction of the error covarience:
       $$P^-_k = AP_{k-1}A^T + Q$$

2) Measurement update equations
   c) Computing the Kalman filter gain:
       $$K_k = P^-_k H^T (HP^-_k H^T + R)^{-1}$$
   d) Correct the state prediction (a) with updated measurement:
       $$\hat{x}_k = \hat{x}^-_k + K_k(z_k - H\hat{x}^-_k)$$
   e) Update error covariance:
       $$P_k = (I - K_k H)P^-_k$$

The state of the marker tracked in the experiment, and a linear system of equations describing the velocity and position in a matrix form can be written as follows:

$$q_k = \begin{bmatrix} x_t \\ \dot{x}_t \end{bmatrix} = \begin{bmatrix} 1 & T \\ 0 & 1 \end{bmatrix} \begin{bmatrix} x_{t-1} \\ \dot{x}_{t-1} \end{bmatrix} + \begin{bmatrix} \Delta T^2 \\ \Delta T \end{bmatrix} \ddot{x}_t \qquad (8)$$

Where x_t and $\dot{x}_t$ are the position and the velocity of the tracked object at the time step t.

By comparison of the above equation with (6), we can write

$$A = \begin{bmatrix} 1 & T \\ 0 & 1 \end{bmatrix} \ and \ B = \begin{bmatrix} \Delta T^2 \\ \Delta T \end{bmatrix} \qquad (9)$$

Position tracking performed during the experimental testing is a 2D tracking case with position data acquired for the X and Y coordinates. The Kalman filter was applied separately to X and Y fused coordinates considering them to be one-dimensional tracking problems.

III. Experimental Methodology

The sensor fusion scheme has been validated in experiments. Figure 3 shows a diagram of how the experimental apparatus was utilized. During the experiments, a robotic arm (Denso VS-068) was used to perform 2D movements which were tracked by the webcam and the optical sensor attached to a fixed stand. In order to evaluate the tracking performance, a reference (benchmark) trajectory was acquired using an Optotrak motion capture system with two infrared sensors.

Data acquired by the Optotrak was sampled at 400 Hz with two infrared sensors: a moving body sensor (moving) and a lab frame sensor (stationary). According to the data acquired with the Optotrak, the measurement error was 0.17 (0.02) mm for the moving body sensor and 0.25 (0.001) mm for the lab frame stationary sensor.
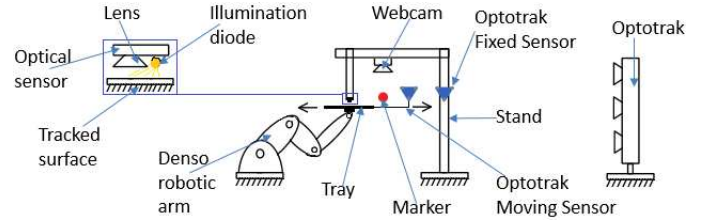

Fig. 3. Schematic diagram of the experimental apparatus.

During experiments, two different trajectories were tracked: a circular trajectory and a pentagram star trajectory. During each experiment, each trajectory was repeated continuously ten times at three different velocities V1 (40 mm/s), V2 (55 mm/s) and V3 (70 mm/s). Position data acquired from the webcam and the optical sensor was fused and filtered using the Kalman filter after the experiments.

IV. Experimental Results

The results presented in this section are for the optical sensor tracking system, the webcam tracking system, and the fusion scheme.

A. Result for optical sensor tracking.

During experiments, a laser diode-illuminated optical sensor (ADNS-9800) was utilized. The mean measured sampling frequency of the optical sensor was 108.4 (21.9) Hz. During experiments three different optical sensor resolutions settings and three different surfaces above which the sensor was used were investigated.

The optical sensor was measuring surface quality (Squal) at each time step. Sqaul is a number from 0 to 676 representing the number of valid features visible by the sensor at the current time step. The higher is the Squal, the more accurate the tracking results. Figure 4 presents mean Squal results for three movement velocities and three resolutions of the optical sensor.
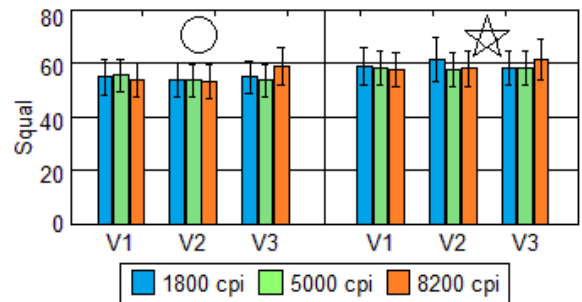

Fig. 4. Optical sensor surface quality (Squal) for circular and pentagram trajectories for three movement velocities and three resolution settings of the optical sensor.

The data presented in Figure 4 shows that there is no clear dependence between the movement velocity and the Squal value. There is also no significant variation between optical sensor resolutions and Squal values. However, it can be noticed that mean Squal values for each optical sensor resolution are higher for the pentagram trajectory movement than for the circular trajectory movement. Table I shows mean Squal values for the three different surfaces types.

Surface type	Gaming mat (c)	Gaming mat (p)	MDF board (c)	MDF board (p)	White paper (c)	White paper (p)
Squal	53.20 (6.38)	57.90 (6.48)	37.81 (4.30)	39.55 (6.94)	36.58 (4.36)	39.24 (6.01)

The data presented in Table I shows that mean Squal values are higher for the pentagram trajectory movement tracking than for the circular trajectory movement tracking for each of the three surfaces. The mean Squal value is the highest for the gaming mat surface – it is more than 40% higher than the mean Squal values for the MDF board. The lowest Squal values were observed for the white paper. Based on the results presented in Table I, the best tracking performance of the optical sensor can be achieved with the gaming mat surface.

Table II shows the dependence between optical sensor drift values per 100 mm travelled and the resolution of the optical sensor. The total drift was calculated as a distance between the start and the end point of the trajectory tracked by the optical sensor. The drift per 100 mm traveled was calculated by multiplying the total drift with 100 mm and dividing by the total distance traveled. The data in Table II indicates that the drift per 100 mm traveled values do not vary significantly with different optical sensor resolutions. However, it can be noticed that the drift values for circular trajectory tracking are double those of pentagram trajectory tracking.

Resolution [cpi]	1800 (c)	1800 (p)	5000 (c)	5000 (p)	8200 (c)	8200 (p)
Drift [mm]	0.30	0.15	0.33	0.16	0.32	0.13

Table III shows the relation between surface type and drift values. As expected, for the pentagram trajectory tracking the lowest drift value (0.16 mm) was recorded for the gaming mat. However, for the circular trajectory tracking the lowest drift value was recorded for MDF board (0.07 mm), whereas a corresponding value for the gaming mat was 0.33 mm. It is difficult to explain the unexpectedly low drift value for the MDF board during circular trajectory tracking. Squal values presented in Table I are lower for the MDF wood than for the gaming mat, therefore it was expected that the drift value for the gaming mat would be the lowest while tracking a circular trajectory. The very low drift value (circular trajectory) for the MDF board can be explained by the fact that the direction of the optical sensor drift changes during movement and in this special case the drift was effectively being cancelled out.

Surface type	Gaming mat (c)	Gaming mat (p)	MDF board (c)	MDF board (p)	White paper (c)	White paper (p)
Drift [mm]	0.33	0.16	0.07	0.75	2.25	1.88

B. Result for webcam tracking.

During the experiments, a standard webcam (Logitech Pro 9000) capable of recording at 30 fps maximum was used. The webcam was mounted on a stand above the tracked object and covering an area 448 by 336 mm, larger than an A3 sheet of paper. The selected resolution was 640 by 480 pixels, therefore 1 pixel was equivalent to 0.7 mm. In order to neutralize the effect of lens distortion, a division calibration method was applied, which reduced the maximum sampling frequency. The mean measured sampling frequency for the webcam was 10 (0.05) Hz. The diameter of the tracked marker (matte red painted ball) was 40 mm. In order to monitor the quality of the recorded data (with the webcam) two parameters were recorded at each time step: average strength (AS) (gradient magnitude of the edge) and radius of the tracked marker. Table IV shows the relation between mean AS values, marker radius and the three velocities. No significant dependence between AS and experimental velocities was observed. The AS values are similar for the circular and pentagram path tracking. However, it can be noticed that the marker radius measurements are more accurate for the circular movement tracking than for the pentagram movement tracking. This suggests that there is an image calibration accuracy problem, which can be solved using a more efficient image calibration method. However, this can lead to an increase in the computational cost of the position calculations.

	V1	V2	V3
Average Strength (c)	0.985 (0.010)	0.985 (0.010)	0.986 (0.010)
Average Strength (p)	0.985 (0.008)	0.987 (0.009)	0.987 (0.009)
Radius mm (c)	19.94 (0.47)	19.94 (0.48)	19.92 (0.49)
Radius mm (p)	19.68 (0.44)	19.67 (0.48)	19.59 (0.51)

C. Results for the fusion of webcam and optical sensor data.

The performance of the fusion tracking scheme was experimentally evaluated. To compute the results trajectories tracked with the Optotrak were used as a benchmark to evaluate the performance of the other tracking systems. Figure 5 presents a comparison between root mean squared errors (RMSE) of the tracking systems at three velocities. Fusion trajectory is based on combined webcam and optical sensor tracked position results, therefore it is significantly dependent on the performance of these two systems. The RMSE values in Figure 5 show that the fusion scheme is benefiting from both the webcam and optical sensor tracking systems. At each velocity, the RMSE value is lower for the fusion scheme when compared to RMSE values for the webcam and the optical sensor. Utilizing the Kalman filter to filter the fused position data did not improve the accuracy of the fusion tracking system. It can be noticed in Figure 5 that RMSE values for the Kalman filter are slightly lower for the circular movement tracking than the corresponding values for the fusion. However, for the pentagram point-to-point movement tracking, the RMSE values for the Kalman filter are higher than the corresponding RMSE values for the fusion. It seems that using the Kalman filter was not significantly beneficial, as the fused tracking data was not very noisy. Utilizing the Kalman filter may be beneficial for tracking movements at velocities higher than the velocities used during the testing or tracking movements with changing acceleration.
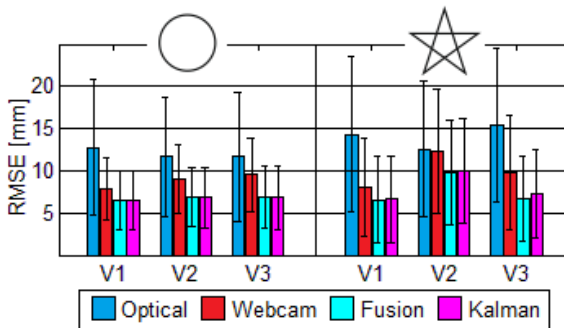
Fig. 5.   Root mean squared error (RMSE) for optical sensor, webcam, fusion scheme and Kalman filter, for circular and pentagram trajectories for three velocities.

Figure 6 presents a sample plot of root mean squared tracking error vs. time for the tracking of a pentagram movement repeated seven times at V3 velocity. It can be observed that the tracking error value for the optical sensor was diverging with time. No significant divergence was observed for the webcam, fusion and Kalman filtered fusion.
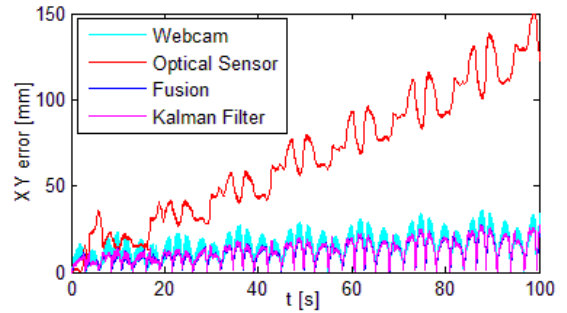
Fig. 6.   Tracking root mean squared error vs time for the pentagram movement tracking at V3 velocity, on a white paper surface.

Figure 7 presents the circular movement tracking results for one full movement repetition (revolution). It grants a closer look at sample plots of X and Y coordinates, surface quality (Squal) measured with the optical sensor, and average strength (AS) together with the marker radius (R) measured with the webcam plotted against the same time scale. It can be seen that the optical sensor measurements diverge and that the trajectory of the fusion scheme is similar to the Optotrak reference trajectory.
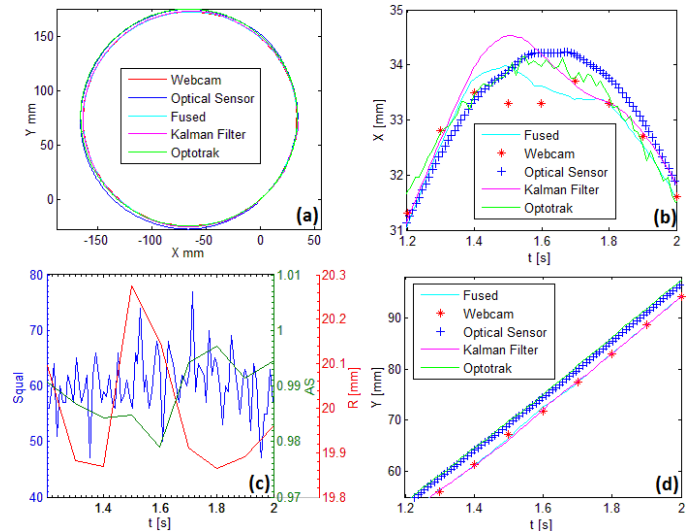
Fig. 7.   Results for the circular movement tracking: one full revolution (a), sample plot of X coordinate vs time (b), sample plot for Squal (optical sensor) and AS and R plots vs time and sample plot of Y coordinate vs time (d).

Similarly, Figure 8 presents the pentagram movement tracking results for one full movement repetition. It grants a closer look at sample plots of X and Y coordinates, Squal, AS and R plotted against the same time scale. In this case, optical sensor measurement divergence is more noticeable than during the circular trajectory tracking. However, once again the trajectory of the fusion scheme is similar to reference trajectory recorded with the Optotrak.
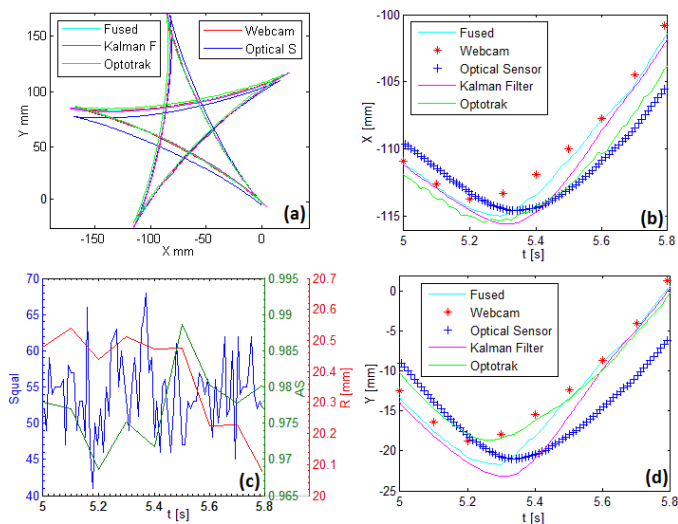
Fig. 8. Results for the pentagram movement tracking: one full repetition (a), sample plot of X coordinate vs time (b), sample plot for Squal (optical sensor) and AS and R plots vs time and sample plot of Y coordinate vs time (d).

V. Discussion

According to the results, fused data from the webcam and the optical sensor can be successfully utilized for position tracking of a passive rehabilitation robot resulting in more accurate position estimates than would be possible if the systems were used on their own. Interestingly, in this case it has been shown that using the Kalman filter did not improve the tracking performance as the tracking trajectory was not very noisy. Instead, a simpler approach using a fusion algorithm with an eight-step correction reduced sudden position data changes during trajectory corrections and provided an effective strategy for position tracking. There are many forms of the Kalman filter which can be implemented, and only the simple discrete Kalman filter was investigated in this work. However, different types of the Kalman filter will be considered in future work if this become necessary. Nonetheless, as long as it performs well, the fusion algorithm will be kept as simple as possible in order to increase computational efficiency.

It has been noticed that the accuracy of position estimations calculated with the fusion algorithm is limited by the quality of absolute and relative position measurements from the webcam and the optical sensor respectively. The accuracy of the webcam positioning is highly dependent on the implementation of a calibration method, whereas the accuracy of the optical sensor positioning varies with different surface types.

The methods employed in this work can be adapted to include the tracking of orientation in addition to linear position. This requires one additional optical sensor and an extension of the fusion algorithm. In its current form, the algorithm cannot be used to track simultaneous changes in an object's position and orientation.

The focus of the work reported here was to evaluate the feasibility and performance of the above techniques under controlled conditions. The trajectories used were representative of human movement in terms of their speed and range of motion. However, to ensure this work is appropriate for use in

the design of home rehabilitation equipment, a key requirement to evaluate these techniques using human participants must be fulfilled. Testing with human participants will reveal the effects of different features of movement such as jerk and spasm on the tracking performance of the system.

VI. Conclusions

A novel type of a position tracking system fusing data from a webcam and an optical sensor was proposed and experimentally evaluated, demonstrating appropriate performance (both temporally and spatially) for use in rehabilitation. The accuracy of the fusion tracking system can be further improved by improving the calibration of the webcam. The proposed fusion tracking system is simple and has the potential to be easily be implemented in a table-top robot designed for home-based upper limb rehabilitation.

References

[1] Morse, Amyas, and Auditor General. "Progress in improving stroke care." (2010).

[2] B. Dobkin, "Strategies for stroke rehabilitation", The Lancet Neurology, vol. 3, no. 9, pp. 528-536, 2004.

[3] N. Norouzi-Gheidari, P. Archambault and J. Fung, "Effects of robot-assisted therapy on stroke rehabilitation in upper limbs: Systematic review and meta-analysis of the literature", The Journal of Rehabilitation Research and Development, vol. 49, no. 4, p. 479, 2012.

[4] G. Kwakkel and C. Meskers, "Effects of robotic therapy of the arm after stroke", The Lancet Neurology, vol. 13, no. 2, pp. 132-133, 2014.

[5] H. Krebs, B. Volpe, D. Williams, J. Celestino, S. Charles, D. Lynch and N. Hogan, "Robot-Aided Neurorehabilitation: A Robot for Wrist Rehabilitation", IEEE Trans. Neural Syst. Rehabil. Eng., vol. 15, no. 3, pp. 327-335, 2007.

[6] S. Coote, B. Murphy, W. Harwin and E. Stokes, "The effect of the GENTLE/s robot-mediated therapy system on arm function after stroke", Clinical Rehabilitation, vol. 22, no. 5, pp. 395-405, 2008.

[7] A. Jackson, M. Levesley, S. Makower, J. Cozens and B. Bhakta, "Development of the iPAM MkII System and Description of a Randomized Control Trial with Acute Stroke Patients", in IEEE International Conference on Rehabilitation Robotics, 24-26 June, 2013.

[8] R. Loureiro, W. Harwin, K. Nagai and M. Johnson, "Advances in upper limb stroke rehabilitation: a technology push", Med Biol Eng Comput, vol. 49, no. 10, pp. 1103-1118, 2011.

[9] S. Housman, K. Scott and D. Reinkensmeyer, "A Randomized Controlled Trial of Gravity-Supported, Computer-Enhanced Arm Exercise for Individuals With Severe Hemiparesis", Neurorehabilitation and Neural Repair, vol. 23, no. 5, pp. 505-514, 2009.

[10] A. Peattie, J. Wilson and B. Sandilands, "Automated Variable Resistance System for Upper Limb Rehabilitation", in Australasian Conference on Robotics and Automation, Sydney, 2009.

[11] J. Perry, H. Zabaleta, A. Belloso, C. RodrÃguez-de-Pablo, F. Cavallaro and T. Keller, "ArmAssist: development of a functional prototype for at home telerehabilitation of post-stroke arm impairment", in The Fourth IEEE RAS/EMBS International Conference on Biomedical Robotics and Biomechatronics, Rome, 2012.

[12] D. Luo, T. Schauer, M. Roth and J. Raisch, "Position and Orientation Control of an Omni-Directional Mobile Rehabilitation Robot", in IEEE International Conference on Control Applications, 2012.

[13] J. Kowalczewski, E. Ravid and A. Prochazka, "Fully-Automated Test of Upper-extremity Function", in 33rd Annual International Conference of the IEEE EMBS, Boston, 2011.

[14] G. Welch and G. Bishop, An Introduction to the Kalman Filter. University of North Carolina at Chapel Hill, 2001, pp. 20-2